Vacuum 148 (2018) 131–135

Contents lists available at ScienceDirect

Vacuum

journal homepage: www.elsevier.com/locate/vacuum

Mitigating target degradation in sputtering manganite thin films

I.M. Dildar[*, 1], D.B. Boltje, M.B.S. Hesselberth, C. Beekman [2], J. Aarts

Kamerlingh Onnes Laboratorium, Leiden University, The Netherlands

ARTICLE INFO

Article history:
Received 9 August 2017
Received in revised form
6 November 2017
Accepted 9 November 2017
Available online 11 November 2017

Keywords:
Epitaxial growth
Sputtering
Atomic force microscopy (AFM)
Heterostructures

ABSTRACT

In this paper, we address the issue of aging of oxide sputtering targets, using the example of $La_{0.7}Ca_{0.3}MnO_3$ (LCMO), a material which is quite sensitive to the amount of oxygen. After prolonged use we find that the morphology of the films becomes poor: holes appear, the size of the steps between terraces becomes larger, the roughness increases, and electrical conductance in the metallic state at temperatures below the metal-insulator transition becomes smaller. We have performed experiments on reactive sputtering with water vapor in order to reverse their degradation. We discuss the growth and properties of films of LCMO on flat $SrTiO_3$ substrates before and after the target treatment. We study both the morphological and structural changes in these films as well as the transport properties. The results indicate that a correct concentration of oxygen in the targets is important, and that a deficiency can be compensated by the water treatment, thus increasing the usable life time of targets.

1. Introduction

Among the family of manganites, $La_{0.7}Ca_{0.3}MnO_3$ is a prototype perovskite manganite which shows a 'colossal' magnetoresistance (CMR) effect near its metal-insulator (MI) transition [1]. It has been much researched to understand the phenomenon of phase separation [2], while the large magnetoresistance and the 100% spin polarization [3] are properties with potential in technological areas such as magnetic storage. The narrow bandwidth of the material makes it very sensitive to hydrostatic pressure [4–6], lattice strain [7,8], doping level [9] and oxygen stoichiometry [10,11]. Especially for thin films, this sensitivity requires optimal parameters in order obtain epitaxial growth and a well-defined MI transition.

We have been growing high quality thin films of $La_{0.7}Ca_{0.3}MnO_3$ by reactive dc sputtering at a high pressure (of order 3 mbar) of oxygen. With passage of time, and without changing the growth parameters, the films became poor in quality. Such behavior is reminiscent of similar problems observed in sputter growth of films of $YBa_2Cu_3O_{7-\delta}$, which was suggested to be due to oxygen depletion of the target surface [12,13]. The addition of water vapor appeared to remedy this situation by increasing the amount of available atomic oxygen [13,14] during growth. A valid discussion on the production of OH radicals in the oxygen-water environment [15] is an associated research line but the issue has not been touched in the present paper. Here we show that adding water vapor in a controlled way during growth results in films with proper morphology, structure and transport properties, even when grown with an old and presumably oxygen deficient target. Hence, this technique can usefully extend the lifespan of sputtering targets of complex oxides.

2. Experiment

Epitaxial thin films of $La_{0.7}Ca_{0.3}MnO_3$ with thickness ranging from 7 nm to 75 nm were grown on flat $SrTiO_3$(001) (STO) substrates using a dc reactive sputtering at an oxygen pressure $p_{O_2} = 3$ mbar. Experiments involving such films were described before [16]. Some necessary description are included here for interest.

A schematic front view of the sputtering system is shown in Fig. 1. A rotary feedthrough is connected to the center of the top flange, which can be lifted up by an electrical motor. A cross-piece with electrical and water feedthroughs, a plate with quartz crystal and heater element are connected to the rotary feedthrough. The substrate heater is surrounded by a cooling shroud to prevent the system and the temperature sensitive pressure gauges from temperature fluctuations. Four sputtering guns are mounted facing upward and the substrate heater can be rotated to be on on-axis

* Corresponding author.
E-mail address: ishratmubeen@gmail.com (I.M. Dildar).
[1] Present address: Department of Physics, University of Engineering and Technology, Lahore, Pakistan.
[2] Present address: Department of Physics, Florida State University, Tallahassee, USA.

https://doi.org/10.1016/j.vacuum.2017.11.016
0042-207X/

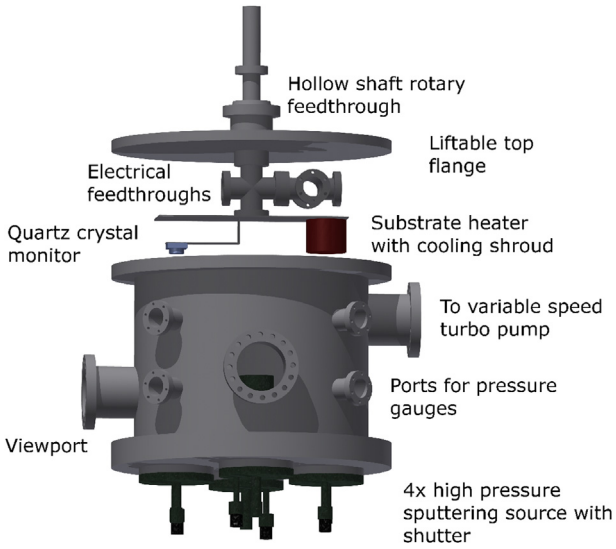

Fig. 1. A 3d schematic view of the oxide sputtering system.

with the each available cathode [17]. Conducting targets of size 2 inches with nominal composition of $La_{0.7}Ca_{0.3}MnO_3$ (LCMO) were purchased from commercial companies with a purity of 99.9% and density better than 96%. In DC sputtering, the targets are pre-sputtered at 1 mbar at a current of 100 mA and then deposition is done at a current of 350 mA at 3 mbar.

The oxide sputtering system was evacuated below pressure 10^{-6} mbar before filling the chamber with oxygen. The target was cleaned and pre-sputtered for one hour to obtain a stable surface composition and to optimize the stoichiometry of the target surface. The substrate was glued on a stainless steel heater (Inconel) using conducting silver paste. Uniformity of the substrate temperature was assured by gluing four STO side plates around the substrate. The temperature was measured with a thermocouple inserted into the heater and regulated to 840 ± 1 °C by an automated Eurotherm temperature controller. A small reservoir filled with water was connected to the vacuum chamber via an electronically controlled leak valve. The system was stabilized at a certain water pressure for about one hour before the process of pre-sputtering and deposition was started. For some films, the leak valve was closed before the deposition was started, which increased the growth rate. The surface morphology of the films was analyzed by Atomic Force Microscopy (AFM). Thickness and lattice parameters were measured by x-ray diffraction (XRD) with Cu-Kα radiation. High resolution XRD (Reciprocal Space Mapping) was performed with a Bruker D8 Discoverer, equipped with a monochromator ($\lambda = 1.5406$ Å) and a Vantec −1 array detector at Twente University. A Physical properties measuring system (PPMS), (temperature range 2–400 K and magnetic field up to 9 T) was used to measure the transport properties of unstructured thin films with silver paint contacts and a four-point in-line geometry, and a distance of 1 mm between the voltage contacts. External voltage and current sources were used to measure the resistance. We found that the optimal water pressure at which good quality thin films were produced was around 5×10^{-5} mbar. Below this pressure, films still showed holes and above this pressure the film surface was not smooth.

3. Results

We compare the intrinsic properties of the films when grown using a relatively new target and grown using an older target with and without adding water vapor to the system. Thin films of $La_{0.7}Ca_{0.3}MnO_3$ grown on $SrTiO_3$ have characteristic features which can be distinguished by Atomic Force Microscopy (AFM) and transport properties. The mismatch between LCMO (pseudocubic lattice parameter $a_{LCMO} = 3.863$ Å) and substrate ($a_{STO} = 3.905$ Å) is −1%, leading to strained films. They still can be flat, with unit cell steps between terraces reflecting the underlying substrate. In thick films, structural defects appear, the roughness increases and steps are not visible anymore.

Fig. 2a shows the topography of a 15 nm thin film of LCMO on STO grown with a fresh LCMO target. The film shows unit cell step height (Fig. 2b). A detailed structural and interface analysis by HRTEM and EELS of such films is given elsewhere [7,8]. The transition temperature (the temperature at which material goes from metal to insulator, for abberation has been written as T_{MI}, temperature showing metal insulator transition) dependence of the resistance of such films is shown in Fig. 3 for thicknesses of 75 nm and 11 nm, both for zero applied magnetic field and in 9 T. The temperature T_{MI} for the 75 nm film is about 190 K, still below the single crystal value 270 K as shown in Fig. 3. For the 11 nm film T_{MI} has decreased to 130 K. Such a drop is a well known effect of tensile strain [8].

We observed that the film properties started to deteriorate with the passage of time without changing the growth parameters i.e., the growth pressure, growth temperature, target to substrate distance, and flow of oxygen. One of the films in this series, with a thickness of 13 nm, is shown in Fig. 4a. The growth time for this film is the same as for the 15 nm thick film shown in Fig. 2a, indicating that the growth rate had increased by about 15%. The surface shows a structure of poorly not well connected grains and holes as dark spots. The profile (Fig. 4b) shows a non-homogeneous film with grain sizes of 20 nm. The root-mean-square surface roughness of this film is 5 nm.

The transport properties of the film, given in Fig. 5 show an MI transition at 100 K, but the metallic state does not fully develop and the resistance increases again below 50 K. Other films grown with a deteriorating target show two or three resistance peaks (not shown here), indicating that these films do not have the typical properties of strained LCMO thin films.

It is known that in particular the correct oxygen content is an important ingredient for bulk CMR manganites [18–23], and that deficiency of oxygen content can influence the crystalline structure, transport and magnetic properties of thin films [24,25]. Oxygen deficient films can be very rough and highly resistive, and in particular decreasing the oxygen amount leads to a lower T_{MI} and an increase in the metallic state resistance [11].

Assuming a possible loss of oxygen in the LCMO target, we

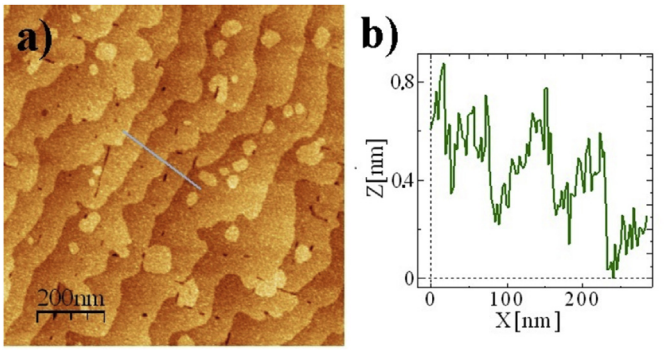

Fig. 2. (a) Surface morphology of a 15 nm thin film of LCMO (L561) grown with a new target shows flat terraces. (b) The height profile shows unit cell high steps of 0.4 nm and the average roughness of the film is 0.2 nm.

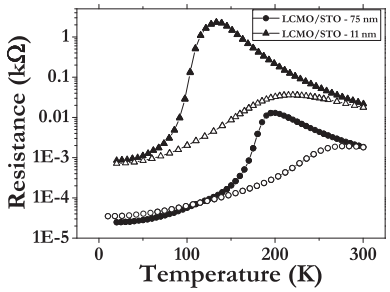

Fig. 3. Temperature dependence of resistance for as grown films of LCMO on STO grown with a new target, a 75 nm film (circles) and a 11 nm thin film (triangles). Filled symbols represent the temperature versus resistance behavior at 0 T and open symbols at 9 T.

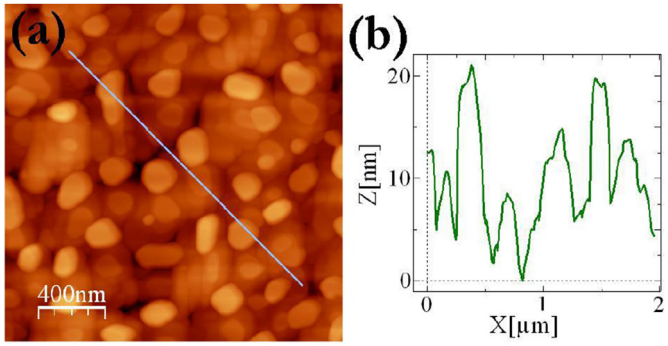

Fig. 4. (a) Surface morphology of a 13 nm thin film of LCMO (L579) grown with a relatively old target (b) The height variation is 20 nm and rms roughness is 5 nm.

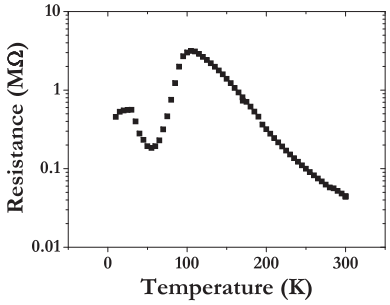

Fig. 5. Temperature dependence of resistance of a 13 nm film of LCMO on STO (L579) grown with a relatively old target, the morphology of the same film is shown in Fig. 4.

attempted to increase the amount of available oxygen by introducing water vapor. A small reservoir of water was connected to the vacuum chamber which could be controlled by a power supply. We grew thin films at three different water pressures and found significant variations in morphology and structure. We use three representative films, denominated in Table 1, to explain the growth of LCMO films at these water pressures.

Fig. 6 shows the AFM data of the three films grown at the water pressures given in Table 1. These pressures are henceforth called P1, P2, P3. The film grown at P1 is smooth but it shows some decorated outgrowth, following the steps of the substrate. The step size is also higher than 2 nm. The film grown at P2 is quite rough, with a rather particular grain structure. The film grown at P3 shows flat terraces with a roughness of 0.2 nm.

The thickness of the films was measured by X-ray Reflectivity (XRR). For the film at P1, fringes could not be found. We used XRD for structural analysis of the films. The diffraction plane (002) can only be found for the films grown at P3 while for the other films, no film peak was found. A 10 nm film, grown after presputtering with water pressure P3 but without water vapor present during growth, also showed good morphology and was analyzed by reciprocal space mapping around the reflection (123), as shown in Fig. 7. The peak of the film can be seen above the substrate peak which is the bright spot at the center. The out-of-plane lattice constant determined with this reflection is 0.382 nm. The in-plane peak values for film and substrate are the same, both 0.39 nm, which shows that the film is epitaxial and strained.

Fig. 8 shows the resistance versus temperature for the three

Table 1
Deposition parameters at different water pressures to optimize the growth of thin films of LCMO. Given are the pressures used to set the water content represented by P_{water} mbar and values are written in mPa in brackets, the process identifier ID (also used to discuss the film properties), the roughness in nm, the thickness of the film d_{LCMO} (nm), and the sample identifier.

P_{water} (mbar)	Process ID	Roughness (nm)	Growth Time (Min.)	d_{LCMO} (nm)	Sample ID
1×10^{-4} (10 mPa)	P1	2	18	x	L580
1×10^{-5} (1 mPa)	P2	2	18	10	L581
5×10^{-5} (5 mPa)	P3	0.4	17	12	L587

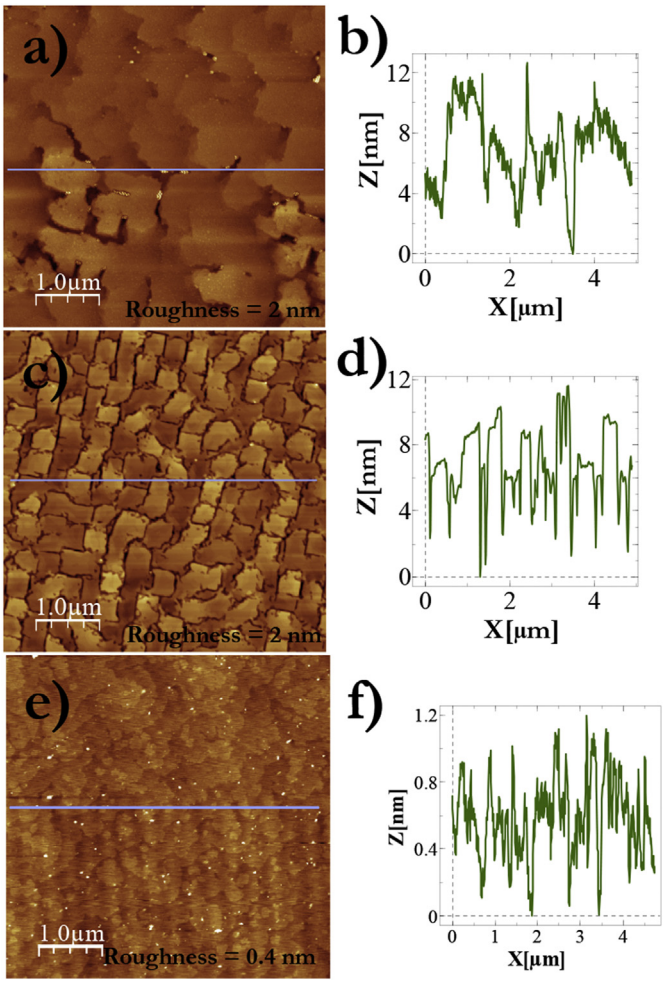

Fig. 6. Effect of different water vapor pressures on the morphology of thin films of LCMO. (a,b) Film L580, grown at 10^{-4} mbar water (P1); (c,d) Film L581 grown at 10^{-5} mbar water (P2); (e,f) Film L587, grown at 5×10^{-5} mbar water (P3).

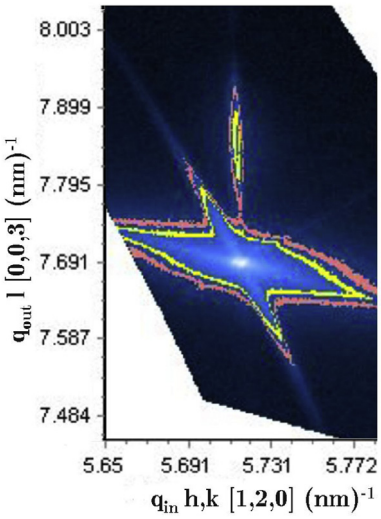

Fig. 7. A reciprocal space map of 10 nm thick LCMO film on STO (L589) around the [123] reflection grown after presputtering with water pressure P3 but without water vapor present. The film peak can be seen at 7.85 nm^{-1}.

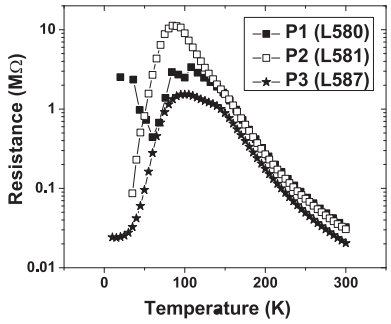

Fig. 8. Transport properties of thin films of LCMO on STO (001) after treatment of target under different water pressures (see Table 1).

films, and only the film at P3 shows a clear MI transition with a drop in resistance of two orders of magnitude. The value of 100 K for T_{MI} is not unusual for this low thickness [26]. The film L589 of which the RSM is given in Fig. 7 even showed a change of four orders of magnitude (not shown). The water vapor pressure of 5×10^{-5} mbar water pressure therefore appears to be optimal, but the result also shows that the window for optimalization is rather small.

We also tested film growth by pre-sputtering the target in the presence of water but closing the water supply before deposition. The films grown in this way showed good morphology, crystallinity, and the correct transition temperature for its thickness. The only difference observed was that films which were grown with water have lower growth rate than done only by conditioning (pre-sputtering in water). Moreover, we also tested the effects of additional water vapor for deposition on substrates of LSGO(001) and on NGO(011), where it worked equally well. The process did not work for substrates with a higher miscut angle (1^o misaligned STO(001)) or a different orientation of surface (STO(110)). We surmise that the different terrace width or orientation leads to a different growth process, which would require optimizing the growth temperature and water pressure to different values.

4. Discussion and conclusion

On the basis of the comparison between the different thin film sets, one grown using a fresh target, one using a degraded target, and one using a degraded target in the presence of water vapor, we conclude it is likely that the mechanism which produces degraded films is the same as was surmised by Krupke et al. for the case of YBCO [13]. A reduced amount of oxygen in the target translates to films with a lack of oxygen, and the addition of water vapor produces atomic oxygen which is easily captured during growth. It is interesting to note in this respect that signs of target degradation can also be found in a decrease of the discharge voltage at constant current and pressure. In our case, at a current of 300 mA, the voltage decreased in time from 380 V for a fresh target to about 364 V when only degraded films were produced. The mechanism is also plausible in view of the findings of Kaufmann and Kelso [27] who showed that the dissociation of O_2 in a microwave discharge is almost entirely due to nitrogenous and hydrogenous impurities.

If one looks at the numbers it becomes clear that water can have such an effect. A current of 300 mA on a 50 mm target results in 10^17 ions/cm^2 impacting the target. This is about the number of surface atoms in a Perovskite. So at the given growth condition only part of a unit cell height is removed from the target every second. In contrast to oxygen, water is known to have a long sticking time at the surface. At 0.0001 mbar each unit cell will experience about 100 collisions every second with a water molecule but only few layers are removed. This means that the target surface will remain saturated with water during the process. It is the ion induced chemical process that, in combination with the sputtering, that compensates for the loss of stoichiometry in the target.

Our experiments show that the water vapor can be either used during growth, in which case the atomic oxygen produced may directly find its way into the growing film; or it may be used to condition the target surface. During growth, the window for the water vapor pressure is rather narrow and needs to be optimized for good results.

Acknowledgments

We thank Dr. Sybolt Harkema for performing high-resolution x-ray diffraction measurements. This research was funded in part by the Foundation for Fundamental Research on Matter (FOM), which is part of the Netherlands Organisation for Scientific Research (NWO). I. M. D. was supported by the Higher Education Commission (HEC) of Pakistan and was on study leave from the University of Engineering and Technology, Lahore, Pakistan.

References

[1] S. Jin, T.H. Thiel, M. McCormack, R.A. Fastnacht, R. Ramesh, L.H. Chen, Thousandfold change in resistivity in magnetoresistive La-Ca-Mn-O films, Sci 264 (1994) 413.
[2] M. Fäth, S. Freisem, A.A. Menovsky, Y. Tomioka, J. Aarts, J. Mydosh, Low temperature magnetoresistance and the magnetic phase diagram of $La_{1-x}Ca_xMnO_3$, Sci 285 (1999) 1540.
[3] R.J. Soulen Jr., J.M. Byers, M.S. Osofsky, B. Nadgorny, T. Ambrose, S.F. Cheng, P.R. Broussard, C.T. Tanaka, J. Nowak, J.S. Moodera, A. Barry, J.M.D. Coey, Sci 282 (1998) 85.
[4] H.Y. Hwang, T.T.M. Palstra, S.-W. Cheong, B. Batlog, Pressure effects on the magnetoresistance in doped manganese perovskites, Phys. Rev. B 52 (21) (1995-I) 15046.
[5] J.J. Neumeier, M.F. Hundley, J.D. Thompson, R.H. Heffner, Substantial pressure effects on the electrical resistivity and ferromagnetic transition temperature of $La_{1-x}Ca_xMnO_3$, Phys. Rev. B 52 (10) (1995) R7006.
[6] Y. Ding, D. Haskel, Y.C. Tseng, E. Kaneshita, M. Veenendaal, J.F. Mitchell, S.N. Sinogeikin, V. Prakapenka, H.K. Mao, Pressure-induced magnetic transition in manganite $La_{0.7}Ca_{0.25}MnO_3$, Phys. Rev. Lett. 102 (2009) 237201.
[7] J. Aarts, S. Freisem, R. Hendrix, H.W. Zandbergen, Disorder effects in epitaxial thin films of (La,Ca)MnO_3, Appl. Phys. Lett. 72 (1998) 2975.
[8] Z.Q. Yang, R. Hendrix, J. Aarts, Y.L. Qin, H.W. Zandbergen, Properties and microstructure of ultrathin (La,Ca)MnO_3 films under different conditions of strain, Phys. Rev. B 70 (2004) 174111.
[9] D.C. Worledge, L. Mieville, T.H. Geballe, On-site Coulomb repulsion in the

small polaron system $La_{1-x}Ca_xMnO_3$, Phys. Rev. B 57 (24) (1998) 15267.
[10] W. Prellier, M. Rajeshwari, T. Venkatesan, R.L. Greene, Effects of annealing and strain on $La_{1-x}Ca_xMnO_3$ thin films: a phase diagram in the ferromagnetic region, Appl. Phys. Lett. 75 (10) (1999) 1446.
[11] K. Dorr, J. M De Teresa, K-H Muller, D. Eckert, T. Walter, E. Vlakhov, K. Nenkov, L. Schultz, Preparation and properties of epitaxial $La_{1-x}Ca_xMnO_{3-\Delta}$ films with reduced carrier density, J. Phys. Condens. Matt 12 (2000) 7099–7109.
[12] R. Krupke, Z. Barkay, G. Deutscher, On the origin of hole formation in YBCO films, Phys. C 289 (1997) 146.
[13] R. Krupke, Z. Barkay, G. Deutscher, A systematic approach to reduce macroscopic defects in c-axis oriented YBCO films, Phys. C 315 (1999) 99.
[14] J.R. Gavaler, J. Talvacchio, T.T. Braggins, M.G. Forrester, J. Greggi, Critical parameters in the single target sputtering of $YBa_2Cu_3O_7$, J. Appl. Phys. 70 (1999) 4383.
[15] S. Yao, S. Weng, Y. Tang, C. Zhao, Z. Wu, X. Zhang, S. Yamamoto, S. Kodama, Characteristics of OH production by O_2/H_2O pulsed dielectric barrier discharge, Vacuum 126 (2017) 16–23.
[16] I.M. Dildar, C. Beekman, X. He, J. Aarts, Hall effect measurements on strained and unstrained thin films of $La_{0.7}Ca_{0.3}MnO_3$ and $La_{0.7}Sr0.3MnO_3$, Phys. Rev. B 85 (2012) 205103.
[17] S. Freisem, PhD thesis, University Leiden, the Netherlands (1999).
[18] C. Ritter, M.R. Ibarra, J.M.D. Teresa, P.A. Algarabel, C. Marquina, J. Blasco, J. Garcia, S. Oseroff, S.-W. Cheong, Influence of oxygen content on the structural, magnetotransport, and magnetic properties of $LaMnO_{3+\delta}$, Phys. Rev. B 56 (1997) 8902.
[19] Z.L. Wang, J.S. Yin, Y.D. Jiang, J. Zhang, Studies of Mn valence conversion and oxygen vacancies in $La_{1-x}Ca_xMnO_{3-y}$ using electron energy-loss spectroscopy, Appl. Phys. Lett. 70 (1997) 3362.
[20] N. Malde, P.S.I.P.N. de Silva, A.K.M.A. Hossian, L.F. Cohen, K.A. Thomas, J.L. MacManus-Driscoll, N.D. Mathur, M.G. Blamire, Influence of oxygen stoichiometry on Raman phonon spectroscopy, lattice parameters and physical properties of $La_{0.7}Ca_{0.3}MnO_3$ thin films, Solid State Commun. 105 (1998) 643.
[21] J. Li, C.K. Ong, J.-M. Liu, Q. Huang, S.J. Wang, Oxygen-deficiency-activated charge ordering in thin films, Appl. Phys. Lett. 76 (2000) 1051.
[22] R. Cauro, A. Gilabert, J.P. Contour, R. Lyonnet, M.-G. Medici, J.-C. Grenet, C. Leighton, I.K. Schuller, Persistent and transient photoconductivity in oxygen-deficient $La_{2/3}Sr_{1/3}MnO_{3-\delta}$ thin films, Phys. Rev. B 63 (2001) 174423.
[23] X.F. Song, G.J. Lian, G.C. Xiong, Small polaronic transport in oxygen-deficient $La_{0.7}Ca_{0.3}MnO_{3-\delta}$ thin films, Phys. Rev. B 71 (2005) 214427.
[24] M. Rajeswari, R. Shreekala, A. Goyal, S.E. Lofland, S.M. Bhagat, R.P. Sharma, R.L. Greene, R. Ramesh, T. Venkatesan, T. Boettcher, Appl. Phys. Lett. 73 (1998) 2672.
[25] S.J. Liu, J.Y. Juang, J.-Y. Lin, K.H. Wu, T.M. Uen, Y.S. Gou, Nonlinear current-voltage characteristics of oxygen-deficient $La_{0.67}Ca_{0.33}MnO_{3-y}$ films, J. Appl. Phys. 103 (2008) 023917.
[26] C. Beekman, J. Zaanen, J. Aarts, Nonlinear mesoscopic transport in a strongly cooperative electron system: the $La_{0.67}Ca_{0.33}MnO_3$ microbridge, Phys. Rev. B 83 (2011) 235128.
[27] F. Kaufmann, J.R. Kelso, Catalytic effects in the dissociation of oxygen in microwave discharges, J. Chem. Phys. 32 (1960) 301.